N78-24050

SUMMARY OF LOW-SPEED AERODYNAMIC CHARACTERISTICS OF UPPER-SURFACE-BLOWN JET-FLAP CONFIGURATIONS

Arthur E. Phelps III
Langley Directorate, U.S. Army Air Mobility R&D Laboratory

Joseph L. Johnson, Jr., and Richard J. Margason
NASA Langley Research Center

4

SUMMARY

The results of recent wind-tunnel investigations to provide fundamental information on the upper-surface-blown (USB) jet-flap concept demonstrated that the USB concept provides good high-lift performance. The low-speed performance appears to be mainly dependent upon the jet turning angle and turning efficiency and on the use of proper leading- and trailing-edge treatment to prevent premature flow separation. The best means of achieving good turning performance in any particular USB application must be determined from overall operational considerations in which high-speed performance, structures and noise, as well as low-speed performance, are evaluated. The large diving moments generated at high lift coefficients can be trimmed satisfactorily with a large, conventional horizontal tail; a high tail position is best from longitudinal stability considerations. Large rolling and yawing moments are introduced with the loss of an engine, but these moments can be trimmed satisfactorily through the use of asymmetrical boundary-layer control and through the use of spoiler and rudder deflection as needed.

INTRODUCTION

In recent years, considerable effort has been directed toward studies of the aerodynamic and acoustic characteristics of upper-surface-blown (USB) jet-flap configurations (refs. 1 to 7). The results of past aerodynamic investigations have indicated that the USB concept can provide the high lift necessary for efficient STOL operation; acoustic studies have indicated that the USB concept may provide beneficial noise reduction during flyovers because the wing shields ground observers from the noise produced at the engine exhaust nozzle. More recent studies have provided solutions to stability and control problems such as pitch trim, longitudinal stability at high lift, and lateral trim for engine-out conditions.

The present paper has been prepared to summarize some of the more important characteristics of USB configurations in the areas of performance, longitudinal stability and trim, lateral-directional stability, engine-out lateral trim, and dynamic stability and control. Although the discussion is directed toward USB configurations, certain problems such as pitch trim and longitudinal stability are common to all powered-lift STOL systems; the problem of engine-out lateral trim is common to other powered-lift concepts utilizing discrete blowing, such as the externally blown flap (EBF) arrangement. Therefore, the data presented

in the present paper for USB configurations may also be generally applicable to other powered-lift concepts.

SYMBOLS

A	aspect ratio
b	wing span
C_L	lift coefficient
C_{L_Γ}	power-induced lift coefficient
$C_{L,max}$	maximum lift coefficient
C_l	rolling-moment coefficient
C_{l_β}	effective dihedral parameter, $\partial C_l/\partial\beta$
C_m	pitching-moment coefficient
C_{m_α}	longitudinal stability parameter, $\partial C_m/\partial\alpha$
C_n	yawing-moment coefficient
C_{n_β}	directional stability parameter, $\partial C_n/\partial\beta$
C_μ	gross thrust coefficient, T/qS
$\bar{c}$	wing mean aerodynamic chord
F_A	axial force
F_N	normal force
l_t	tail length
T	thrust
$T_{1/2}$	time to damp to half-amplitude
W	weight
y,z	body axes coordinates
α	angle of attack
γ	flight path angle
δ_f	flap deflection

δ_j jet deflection

ϵ downwash angle

ω_d Dutch-roll damped frequency parameter

Abbreviations:

BLC boundary-layer control

EBF externally blown flap

USB upper-surface blown

V.G. vortex generator

PERFORMANCE

In a previous paper by William C. Sleeman and Arthur E. Phelps (ref. 8), it was shown that good static turning could be achieved with the USB concept. Figure 1 summarizes the static turning performance of a number of different USB configurations in terms of the ratio of normal force to thrust plotted against the ratio of axial force to thrust. The shaded band in figure 1 indicates representative values of static turning performance obtained with the USB concept and shows that efficiencies from about 80 to 90 percent can be obtained with high flap settings. For lower flap settings, efficiencies are generally much higher (95 percent or greater for flap angles below about 40°) and turning angles are within a few degrees of the upper surface tangency angle.

It has been determined from previous experience that a USB configuration with marginal static turning performance caused by regions of separated or partially separated flow will almost certainly exhibit poor lift performance in forward flight. Good static turning characteristics, on the other hand, have been shown to be a reliable indicator of good lift performance in forward flight. Figure 2 illustrates the effect of forward speed on the static pressure distribution and surface temperatures of a large-scale USB model with turbofan engines (ref. 3). Static turning tests of the configuration indicated good static performance. As shown in figure 2, forward speed had little effect on the magnitudes of the static pressures and surface temperatures along the engine centerline. Forward speed caused only slightly higher suction pressures and slightly cooler temperatures over the flap. Based on these results, it appears that structural and thermal design information may be determined for USB wing-flap systems on the basis of static tests which might be conducted with outdoor static rigs utilizing full-scale engines, nacelles, and wing-flap hardware.

Although tests have shown that the two major externally blown powered-lift concepts (EBF and USB) are generally comparable in overall performance, there are some fundamental differences in the exhaust jet flow fields between the two concepts at forward speed conditions. For example, in the EBF system the jet impinges on the lower surface of the flap and spreads spanwise, covering most

of the flap span. In the USB system, however, a different, more localized flow behavior occurs as indicated in figure 3. The sides, or edges, of the jet sheet produced by the engine exhaust roll up into vortices which enlarge and tend to thicken the jet as it turns over the trailing-edge flap. A number of factors influence the formation of these vortices, but the ratio of jet velocity to free-stream velocity and the thickness of the jet produced by the engine exhaust seem to be the most powerful. In addition to the vortex rollup of the jet sheet, there may be additional vortices produced by the external shape of the USB nozzle. This is especially true for a sharp-cornered rectangular nozzle; the nozzle vortices can be minimized by using a well-rounded or D-shaped nozzle. The overall effect of this vortex formation is to confine the jet influence to a highly localized region near the jet. In fact, the jet may actually entrain free-stream air in such a way as to cause spanwise flow inboard, rather than outboard. The significance of this flow characteristic will be discussed in subsequent sections of this paper.

Figure 4 presents high-lift data for a two-engine straight-wing USB configuration (ref. 4) over a range of Reynolds number and for power-off and power-on cases. The data show the anticipated large influence of Reynolds number on lift for the power-off case, but for the power-on case $(C_\mu = 3)$, the data show very little effect of free-stream Reynolds number. These results have also been observed in other investigations, indicating that for moderate to high thrust coefficients, the lift characteristics of the complete configuration are predominantly influenced by the exhaust jet rather than the free-stream flow; this factor may be related to the high level of turbulence of the jet as it impinges on the wing. From these results, it appears that small-model data may be used with confidence in the design of propulsive-lift systems.

Shown in figure 5 are data illustrating the effect of a leading-edge Krueger flap on the lift characteristics of a USB model with a high jet turning angle $(\delta_f = 60^o)$. The trailing-edge jet turning angle generates a strong upwash field ahead of the wing, and the need for leading-edge devices for adequate protection against leading-edge stall is clearly demonstrated by the data. As can be seen, a marked increase in maximum lift coefficient and in stall angle of attack resulted from the installation of a leading-edge Krueger flap.

One interesting point noted in tests of USB configurations is that close attention must be given to leading-edge stall in the vicinity of the nacelle. The very powerful upwash at the wing leading edge can pose serious problems when the nacelle is close to the fuselage or another nacelle (as in a four-engine arrangement). Figure 6 illustrates this problem for a two-engine straight-wing configuration and a four-engine swept-wing configuration. Both configurations were large-scale wind-tunnel models powered by JT15D-1 turbofan engines to provide a more realistic operational environment than that produced by small, cold jets. During tests of the two-engine straight-wing model (ref. 3), a very strong upwash field was observed between the nacelle and fuselage during power-on conditions. Without leading-edge treatment in this region (which was only about 2 percent of the wing span) the wing inboard of the jet and the entire top surface of the fuselage between the nacelles was badly stalled. Recontouring the lower surface of the nacelle to provide smoother flow transition and adding a leading-edge Krueger flap with blowing BLC between the nacelle and

fuselage resulted in a significant improvement in the flow quality over the fuselage. The left side of figure 6 shows the lift improvements resulting from the modifications to the original wing.

A similar problem was encountered in tests of the large four-engine swept-wing configuration of reference 9 which exhibited severe separation along the leading edge between the fuselage and inboard nacelle and between the inboard and the outboard nacelles. In this case, unsweeping the leading edges, recontouring the lower surface of the nacelles, and adding blown leading-edge Krueger flaps resulted in the improvements shown on the right side of figure 6. These data indicate a significant increase in both $C_{L,max}$ and stall angle of attack for the modified model.

The effects of partial- and full-span flaps on the lift characteristics of a two-engine USB configuration are presented in figure 7. The data show that a large increase in lift coefficient is obtained by extending the trailing-edge flap to full span. In order to determine the proportion of this lift increment due to power effects, the data were analyzed in terms of power-induced circulation lift coefficient C_{L_Γ} as a function of thrust coefficient, and the results are presented in figure 8. The data of figure 8 show that the benefit of power-induced circulation lift on the lift of a USB configuration with full-span flaps is minimal. Also presented in figure 8 are data for an internally blown jet flap in which the exhaust flow is distributed uniformly along the entire wing span (ref. 10). Generally speaking, the localized-flow USB configuration produces about 65 to 70 percent of the power-induced circulation lift available from an internally blown system.

Presented in figure 9 is a plot of the spanwise distribution of normal-force coefficient for the same model used to obtain the lift data of figure 8. The data of figure 9 are presented for power-off, power-on, and engine-out conditions at zero angle of attack. These data indicate that the influence of the exhaust jet on the wing is contained in a region extending approximately 1.75 nozzle widths outboard of the nozzle. In fact, for spanwise locations outboard of the 65-percent-semispan station, the power-off and power-on load distributions are very nearly the same. Of course, the actual spanwise location at which the engine-induced loads diminish to the power-off levels is configuration dependent, but arrangements in which the engines are located well inboard on the wing will generally exhibit this characteristic. From figure 9 it appears that the amount of lift to be gained by deflecting a flap on the outboard portion of the wing (beyond about 70 percent of the semispan) is primarily the lift available from unpowered flow conditions, and it is not likely to be greatly influenced by power-induced effects.

Figure 10 presents the lift characteristics of a number of USB configurations having different nozzle designs. Included are data for rectangular nozzles of three different width-height ratios, a fairly high kickdown D-nozzle; a low kickdown D-nozzle with vortex generators (ref. 11), and a D-nozzle with BLC (hybrid USB, ref. 12). The data presented have been plotted for a jet turning angle of 50°. These data indicate that at low to moderate thrust coefficients, such as those used on approach, there is very little difference in lift for the configurations tested. Thus, it appears that the lift characteristics

of USB configurations may be primarily a function of the jet turning performance, assuming adequate leading- and trailing-edge treatment to prevent premature flow separation. It has been shown (ref. 13) that the geometric nozzle characteristics which are desirable for good turning (such as high-aspect-ratio rectangular nozzles, large kickdown angles, and flare angles) are detrimental to cruise performance. It appears, therefore, that variable geometry features, such as nozzle deflectors or vortex generators, or BLC may be required to achieve optimum performance for both the high-speed and low-speed flight conditions. In any event, the design of a single nozzle to satisfactorily fulfill both the high-speed and low-speed requirements represents a significant challenge to the designer.

The foregoing discussion has centered on the lift performance of the USB concept. However, drag characteristics are also important from an operational viewpoint. A flight envelope relating glide path, lift coefficient, thrust-weight ratio, and angle of attack is very useful in relating lift and drag to overall performance because it serves to establish power requirements and speed margins for a given configuration. Figure 11 presents trimmed flight envelopes for a two-engine straight-wing USB configuration and for a four-engine swept-wing USB configuration. The lift data for these two configurations are contained within the bands shown on figure 10 and are therefore generally representative of USB configurations tested.

At the present time, there are no certified requirements for approach performance of powered-lift airplanes. For the data of figure 11, it is assumed that the aircraft will fly a 7.5° glide slope at a lift coefficient of 4.0. In the event of an engine failure, it must be possible to arrest the descent with full power on the remaining engines without changing flap setting or lift coefficient. From the data on the left side of figure 11 it can be seen that, for the two-engine configuration, the landing approach can be flown at a thrust-weight ratio of 0.21 with a stall margin of about 14°. In order to arrest the descent at this same flap setting, a thrust-weight ratio of 0.35 is required. It has been found with this model and with other USB (and EBF) models that such performance envelopes are almost the same with one engine out as with all engines operating. Hence it can be concluded that, for this two-engine configuration, a total installed thrust-weight ratio of about 0.70 is required.

A similar analysis of the data for the four-engine configuration shown on the right side of figure 11 indicates an approach thrust-weight ratio of 0.25, and an engine-out thrust-weight ratio requirement of 0.45. In the case of the four-engine configuration, only 25 percent of the available thrust is lost in an engine failure, so the four-engine aircraft requires an installed thrust-weight ratio of 0.60.

Based on such analysis, it appears that somewhat higher values of thrust-weight ratio are required for the two-engine configuration than for the four-engine configuration, as would be expected. The data of figure 11 have been found to be generally representative of both USB and EBF configurations; generally, both concepts require higher installed thrust-weight ratios than internally blown flap concepts (such as the distributed blowing concept which distributes the jet uniformly along the wing span). The simplicity of the

discrete-blowing, powered-lift systems, however, make them attractive for application to powered-lift STOL aircraft, as indicated by the selection of the USB and EBF concepts for use in the powered-lift prototype aircraft of the U.S. Air Force Advanced Medium STOL Transport program.

LONGITUDINAL STABILITY AND TRIM

It is a well-known fact that provision of adequate trim in pitch is a serious problem for powered-lift airplane configurations as illustrated in figure 12. The data show the variation of pitching moment with angle of attack for several thrust levels at high lift conditions for a swept-wing, two-engine USB configuration with the horizontal tail off. It should be noted that high thrust increases the longitudinal instability as well as the diving moments of the configuration.

The significance of the large diving moments produced by powered lift in terms of tail size required for trim is shown in figure 13. The figure shows the tail size required for trim as a function of tail lift coefficient following the procedure outlined in reference 14. The tail trim requirements were determined for a maximum wing lift coefficient of 8, a tail length of $3.5\bar{c}$, and a static margin of 10 percent. Figure 13 shows that for a plain elevator, the tail size required for trim is about 37 percent of the wing area, a value nearly double that required by conventional airplanes. The use of a slotted elevator can reduce the required tail size to about 30 percent of the wing area, but a considerably higher tail lift coefficient would be required to reduce the size of the tail to that for conventional airplanes.

The foregoing data have shown that the powered-lift configuration exhibits large pitching moments and that a large tail is required for trim. It should be pointed out that one very important factor which must be considered in sizing the tail is the tail location. As in the case of other powered-lift systems, the high lift generated in the USB concept results in very high downwash angles, particularly directly behind the engines. For this reason, care must be taken in locating the horizontal tail so as to avoid the high downwash region in which the tail could become ineffective. As an example of the flow characteristics behind a USB configuration, the variation of the downwash factor $1 - \frac{\partial \varepsilon}{\partial \alpha}$ with C_L for the two-engine configuration for three vertical locations of the horizontal tail is presented in figure 14. The data in figure 14 are for low-angle-of-attack conditions, and the increase in lift coefficient is obtained by an increase in thrust rather than by an increase in angle of attack. The data of figure 14 show that regardless of the tail location, the tail lost effectiveness as power was increased, but the high tail position was much better than the lower positions.

Flow survey work for USB configurations has not been as extensive as for EBF configurations, so earlier work performed on EBF models was used for guidance with regard to tail location. Stability and control studies of EBF configurations showed that with engines located inboard on the wing, a strong downwash

field was produced along the rear of the fuselage which made the low tail arrangement undesirable from stability considerations. Also, it was found that vortices shed from the wing tips and flaps did not trail straight backward but were drawn in sharply toward the centerline of the airplane. At high angles of attack, a horizontal tail located relatively far rearward and low would enter the vortex flow and become ineffective. For this reason, the horizontal tail was generally located high and forward to retain its stabilizing contributing for higher thrust levels and higher angles of attack. Limited flow survey work with the USB concept has demonstrated downwash characteristics similar to those of EBF concepts, and similar high-forward horizontal tail locations have proven desirable from longitudinal stability considerations.

In order to illustrate how the downwash data of figure 14 affect the contribution of the horizontal tail to stability, calculations have been made to determine the C_{m_α} contribution of the tail at the high and low tail locations of figure 14. The results are shown in figure 15 together with tail-off data. The tail contributions are based on a tail size of 35 percent of the wing area and a tail length of $3.5\bar{c}$. The data show that at low lift coefficients, the high tail position provided adequate stability. The low tail, however, provided very little stability at low lift coefficients and, as the lift coefficient was increased by increasing power, the combined effects of increased instability of the wing-fuselage combination and reduced tail effectiveness resulted in a very unstable configuration at high power settings.

LATERAL-DIRECTIONAL STABILITY

The lateral-directional stability discussion presented herein is based on results obtained for two USB model configurations which were flight tested in the Langley full-scale tunnel. Photographs of the two models mounted for static force tests are presented in figure 16. One model, with an unswept wing and two engines mounted close inboard to the fuselage, represented a 1/5-scale model of the large-scale USB Aero Commander configuration recently tested in the Langley full-scale tunnel. The second model was a four-engine, swept-wing USB configuration. Although the two models were different in planform and engine arrangement, the powered-lift characteristics for the two configurations were generally very similar, as illustrated by the data in figure 17. The lateral-directional stability characteristics for the two models, however, were considerably different, as shown in plots of the directional stability derivative C_{n_β} and the effective dihedral derivative C_{l_β} in figure 18. As shown by the data, the swept-wing configuration had relatively large values of positive effective dihedral which increased as lift coefficient increased. The directional stability was also relatively high and there was an increase in directional stability with increasing lift coefficient. The data for the straight-wing configuration show that the dihedral effect was relatively small and actually decreased with increasing power, but the directional stability increased very rapidly as power was applied. The differences in dihedral effect for the two configurations can probably be attributed to the differences in wing sweep angle. The differences in directional stability were primarily a result of differences

in the effect of the engine exhaust wake on the vertical tail. The engines were located much closer to the fuselage on the straight-wing configuration than on the swept-wing configuration, and the vertical tail was influenced much more by sidewash than on the swept-wing arrangement.

In order to illustrate how these differences in the static lateral-directional stability derivatives affect dynamic lateral-directional stability characteristics, period and damping characteristics were determined by using three-degree-of-freedom calculations for the two models; the results are presented in figure 19. The data show Dutch-roll characteristics in terms of the damping parameter $\frac{1}{T_{1/2}}$ and the damped frequency parameter ω_d. The handling quality boundaries were taken from an AGARD publication for STOL handling criteria (ref. 15). The plot on the left of figure 19 shows that the Dutch-roll oscillation for the swept-wing configuration was unstable and would be considered unacceptable with power off $(C_L = 1.5)$ or on $(C_L = 5.0)$. In order to achieve acceptable Dutch-roll characteristics, the damping in both roll and yaw would have to be doubled; even higher artificial damping would be required for satisfactory characteristics. In contrast to these results, the plot on the right side of figure 19 shows that the Dutch-roll mode for the unswept-wing configuration was stable and that increasing power resulted in increased Dutch-roll damping, with the result that satisfactory characteristics could be achieved without artificial stabilization.

ENGINE-OUT LATERAL TRIM

One of the major problems associated with powered-lift systems utilizing discrete blowing is that of restoring lateral trim in the event of the failure of one engine. This problem involves both roll and yaw, with the roll requirement being the more critical in an approach condition. One major objective of recent research on the USB concept was to determine effective means of providing roll trim for the engine-out condition. One method found to be effective for the USB configuration was that of asymmetrical boundary-layer control, that is, boundary-layer control on the leading edge and on the aileron of the engine-out wing. Some lateral trim data obtained with this method of trim are shown in figures 20 and 21 for the swept-wing and straight-wing flying models.

Figure 20 is a plot of yawing-moment coefficient and rolling-moment coefficient plotted against lift coefficient for the four-engine, swept-wing flying model. In a four-engine operation, the rolling moments were essentially zero and a maximum trimmed lift coefficient of 10 was achieved. With the failure of an outboard engine, the maximum lift coefficient decreased to about 8 and large out-of-trim rolling and yawing moments were introduced. By applying boundary-layer control to the failed engine side, it was possible to simultaneously provide roll and yaw trim. Additional moments produced by spoiler deflection could then be used for maneuver control.

The data of figure 21 show the engine-out rolling-moment and yawing-moment coefficients plotted against lift coefficient for the two-engine, straight-wing

flying model. In this case, the application of boundary-layer control to the failed-engine side reduced the out-of-trim rolling and yawing moments, but it was necessary to employ spoiler deflection and a blown rudder to achieve roll and yaw trim. Additional spoiler and rudder deflection were available for maneuver control.

MODEL FLIGHT TEST RESULTS

As part of the basic research program of USB jet-flap configurations, dynamic stability and control investigations have been made of the four-engine swept-wing configuration and the two-engine straight-wing configuration by using the free-flight model technique. This technique has proved to be useful in previous research in pointing out problem areas which might have been overlooked in conventional testing. The swept-wing model, shown in flight in figure 22, had a span of 3.05 m (10 ft) and was powered by four 13.97-cm-diameter (5.5 in.) turbofan engine simulators driven by compressed air. The horizontal tail incorporated a Krueger flap, and the elevator was deflected upward 50°. Longitudinal control was provided by deflecting the entire horizontal tail, and lateral-directional control was provided by spoilers and rudder. The two-engine straight-wing model was powered by turbofan engine simulators similar to those used on the swept-wing model and had a similar control system.

The free-flight technique is illustrated in figure 23. This figure shows a model being flown without restraint in the 9- by 18-m (30- by 60-ft) open-throat test section of the Langley full-scale tunnel and remotely controlled about all three axes by human pilots. Control surfaces are operated by remotely controlled pneumatic actuators. Pneumatic power and electric control signals are supplied to the model through a flexible trailing cable made up of electrical conductors and light plastic hoses.

The results of the free-flight model tests showed that with all engines operating and with artificial damping about the roll and yaw axes, the models were easy to fly even at lift coefficients up to 8.0. Without artificial stabilization, however, the swept-wing model exhibited a lightly damped Dutch-roll oscillation which made flying difficult. The straight-wing model exhibited good damping characteristics and was easy to fly without artificial stabilization. These results were in good agreement with the previously discussed dynamic stability calculations. With one engine inoperative, the models were trimmed laterally through the use of boundary-layer control on the leading edge and aileron of the engine-out wing and through the use of spoiler and rudder deflection as needed for additional lateral-directional trim. With artificial damping, the models were flown up to high lift coefficients, and the dynamic behavior with one engine inoperative was found to be generally similar to that for all engines operating.

CONCLUDING REMARKS

The results of recent wind-tunnel investigations to provide fundamental information on the upper-surface-blown (USB) jet-flap concept demonstrated that the USB concept provides good high-lift performance. The low-speed performance appears to be mainly dependent upon the jet turning angle and turning efficiency and on the use of proper leading- and trailing-edge treatment to prevent premature flow separation. The best means of achieving good turning performance in any particular USB application must be determined from overall operational considerations in which high-speed performance, structures and noise, as well as low-speed performance, are evaluated. The large diving moments generated at high lift coefficients can be trimmed satisfactorily with a large, conventional horizontal tail; a high tail position is best from longitudinal stability considerations. Large rolling and yawing moments are introduced with the loss of an engine, but these moments can be trimmed satisfactorily through the use of asymmetrical boundary-layer control and through the use of spoiler and rudder deflection as needed.

REFERENCES

1. Phelps, Arthur E.; Letko, William; and Henderson, Robert L.: Low-Speed Wind-Tunnel Investigation of a Semispan STOL Jet Transport Wing-Body With an Upper-Surface Blown Jet Flap. NASA TN D-7183, 1973.

2. Phelps, Arthur E., III; and Smith, Charles C., Jr.: Wind-Tunnel Investigation of an Upper Surface Blown Jet-Flap Powered-Lift Configuration. NASA TN D-7399, 1973.

3. Staff of the Langley Research Center: Wind-Tunnel Investigation of the Aerodynamic Performance, Steady and Vibratory Loads, Surface Temperatures and Acoustic Characteristics of a Large-Scale Twin-Engine Upper-Surface Blown Jet-Flap Configuration. NASA TM X-72794, 1975.

4. Smith, Charles C., Jr.; Phelps, Arthur E., III; and Copeland, W. Latham: Wind-Tunnel Investigation of a Large-Scale Semispan Model With an Unswept Wing and an Upper-Surface Blown Jet Flap. NASA TN D-7526, 1974.

5. Sleeman, William C., Jr.; and Hohlweg, William C.: Low-Speed Wind-Tunnel Investigation of a Four-Engine Upper Surface Blown Model Having a Swept-Wing and Rectangular and D-Shaped Exhaust Nozzles. NASA TN D-8061, 1975.

6. Reshotko, Meyer; Olsen, William A.; and Dorsch, Robert G.: Preliminary Noise Tests of the Engine-Over-the-Wing Concept. I. 30°-60° Flap Position. NASA TM X-68032, 1972.

7. Reshotko, Meyer; Olsen, William A.; and Dorsch, Robert G.: Preliminary Noise Tests of the Engine-Over-the-Wing Concept. II. 10°-20° Flap Position. NASA TM X-68104, 1972.

8. Sleeman, William C., Jr.; and Phelps, Arthur E., III.: Upper-Surface-Blowing Flow-Turning Performance. Powered-Lift Aerodynamics and Acoustics, NASA SP-406, 1976. (Paper no. 2 of this compilation.)

9. Koenig, David G.; and Aoyagi, Kiyoshi: Maximum Lift of Upper Surface Blowing STOL Aircraft With Swept Wings. AIAA Paper No. 75-868, June 1975.

10. Lowry, John G.; Riebe, John M.; and Campbell, John P.: The Jet-Augmented Flap. Preprint No. 715, S.M.F. Fund Paper, Inst. Aeronaut. Sci., Jan. 1957.

11. Wimpress, John K.: Upper Surface Blowing Technology as Applied to the YC-14 Airplane. [Preprint] 730916, Soc. Automot. Eng., Oct. 1973.

12. Carros, Robert J.; Boissevain, Alfred G.; and Aoyogi, Kiyoshi: Aerodynamic Characteristics of a Large-Scale Hybrid Upper Surface Blown Model Having Four Engines. NASA TM X-72460, 1975.

13. Skavdahl, Howard; Wang, Timothy; and Hirt, William J.: Nozzle Development for the Upper Surface-Blown Jet Flap on the YC-14 Airplane. [Preprint] 740469, Soc. Automot. Eng., Apr.-May 1974.

14. Johnson, Joseph L., Jr.: Wind-Tunnel Investigation of the Static Longitudinal Stability and Trim Characteristics of a Sweptback-Wing Jet-Transport Model Equipped With an External-Flow Jet-Augmented Flap. NACA TN 4177, 1958.

15. V/STOL Handling. I - Criteria and Discussion. AGARD Rep. No 577, Dec. 1970.

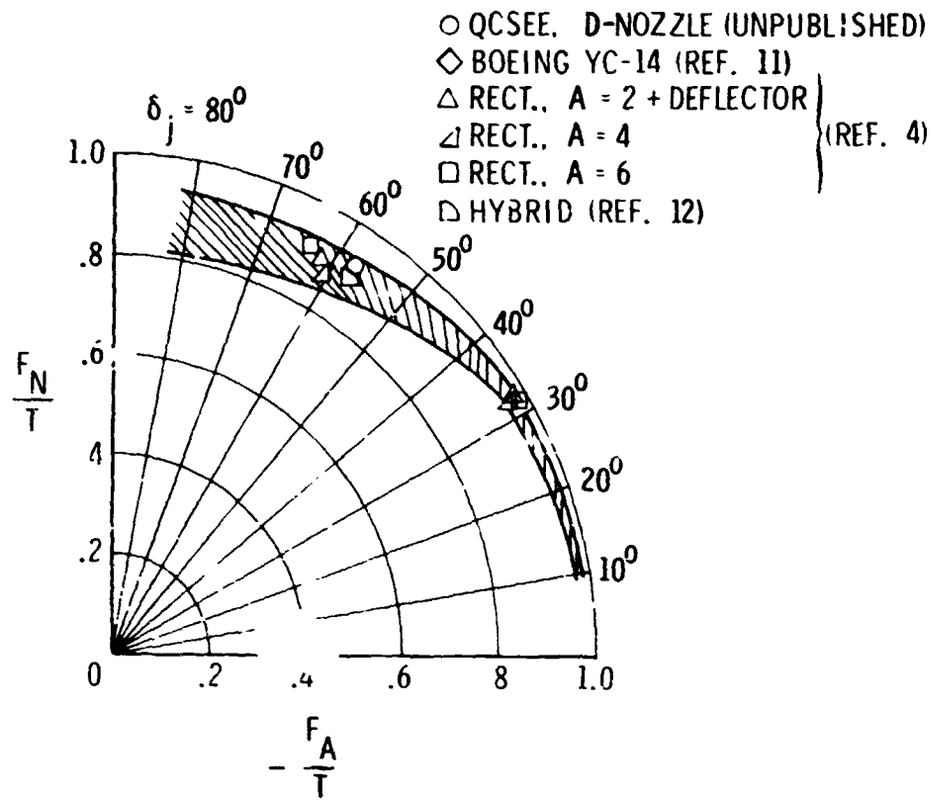

Figure 1.- Static turning characteristics of several USB configurations.

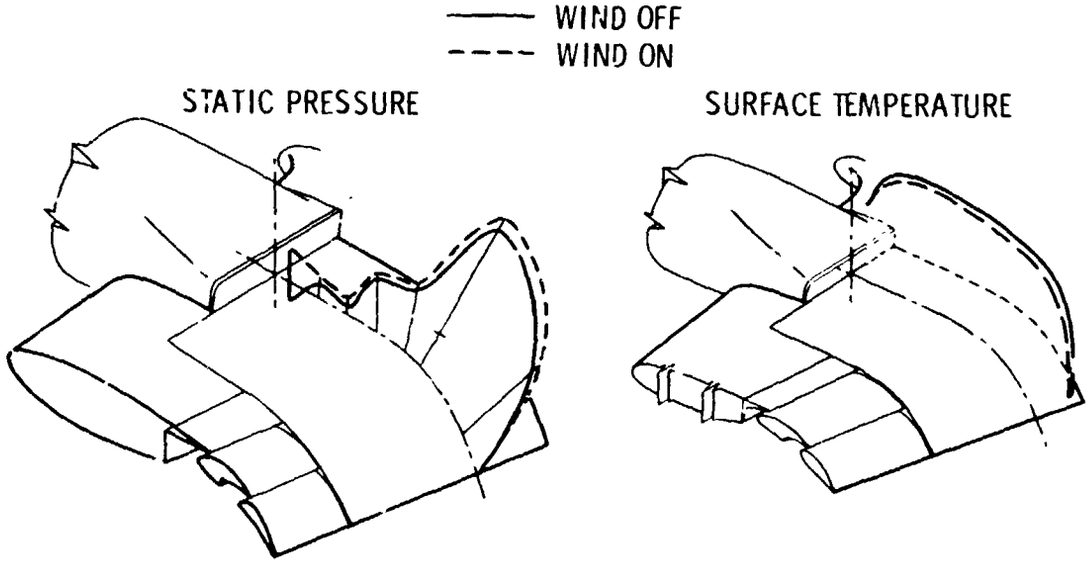

Figure 2.- Pressure and temperature profiles.

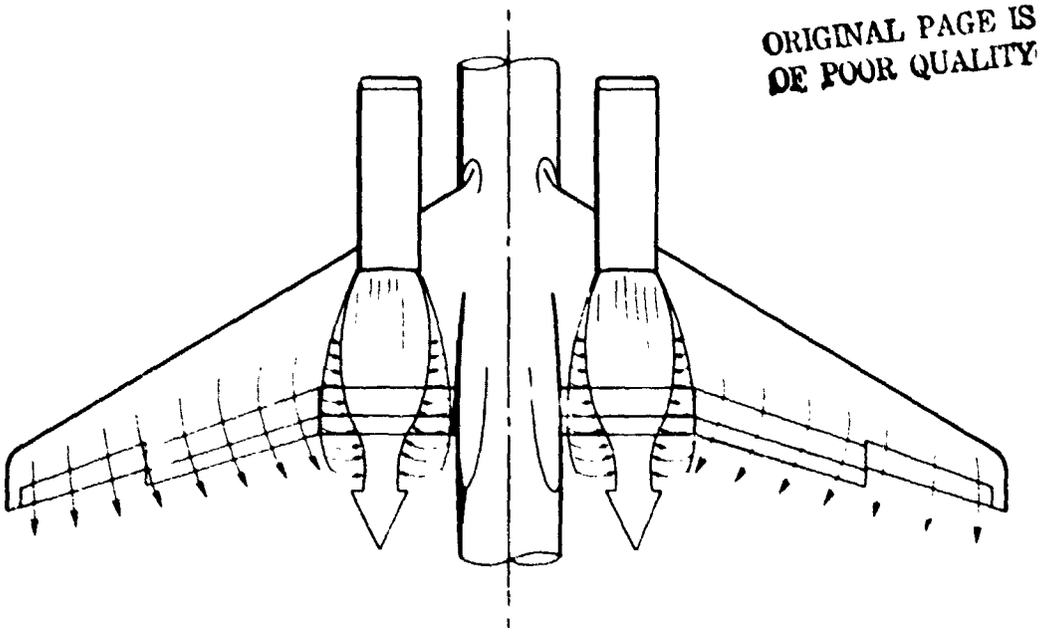

Figure 3.- USB flow characteristics.

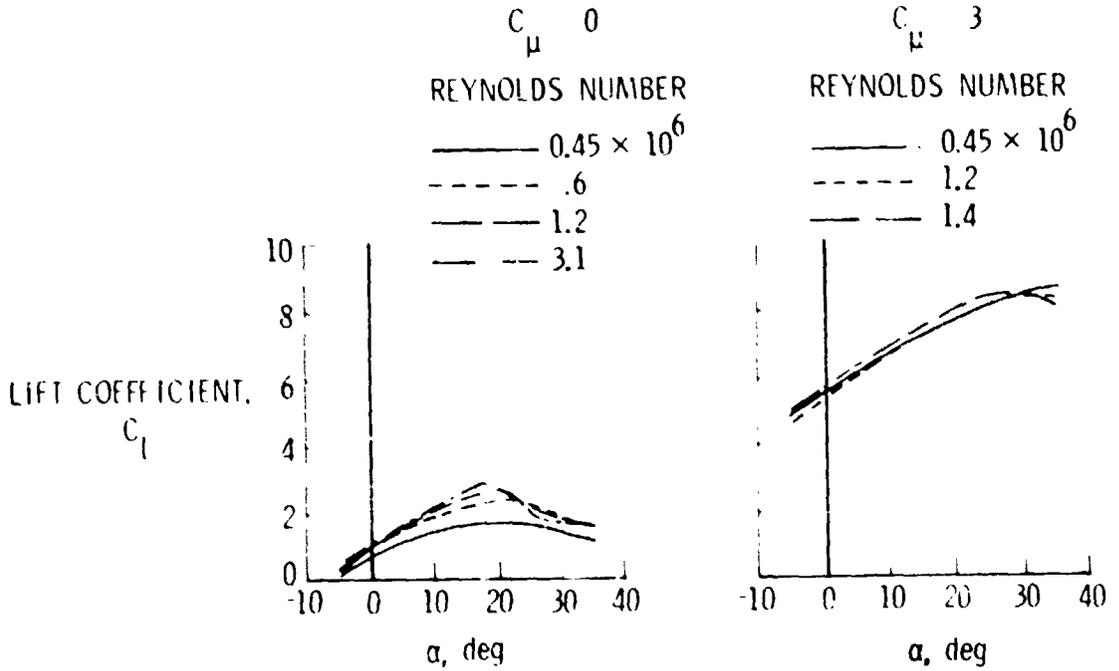

Figure 4.- Effect of Reynolds number on lift characteristics for two-engine straight-wing USB configuration.

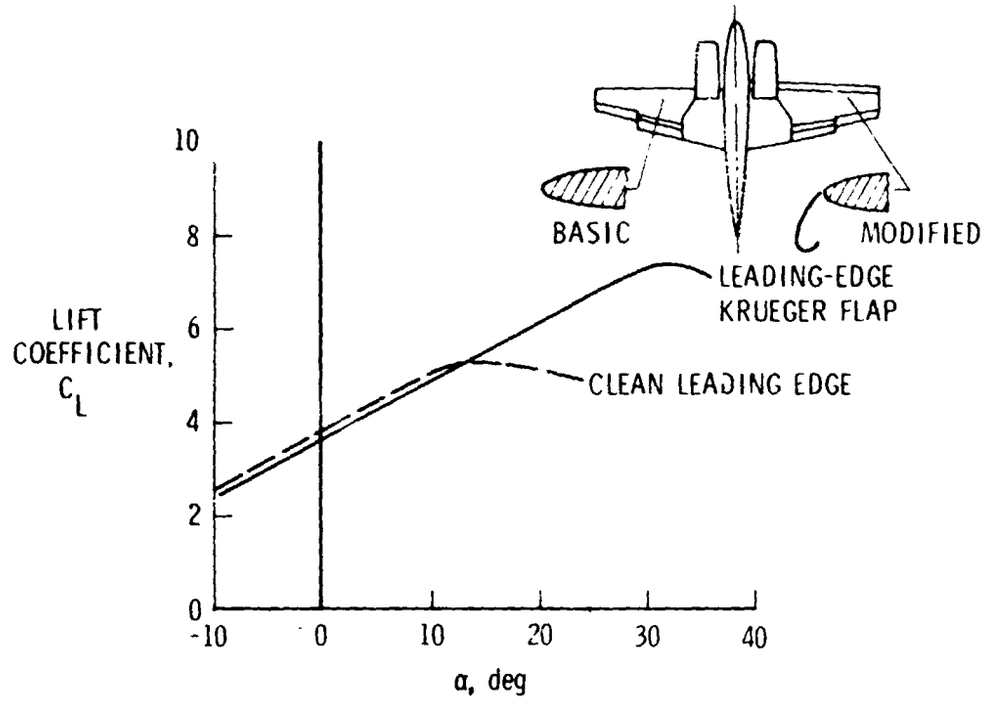

Figure 5.- Effect of leading-edge high-lift devices on lift. $\delta_f = 60^o$; $C_\mu = 2.0$.

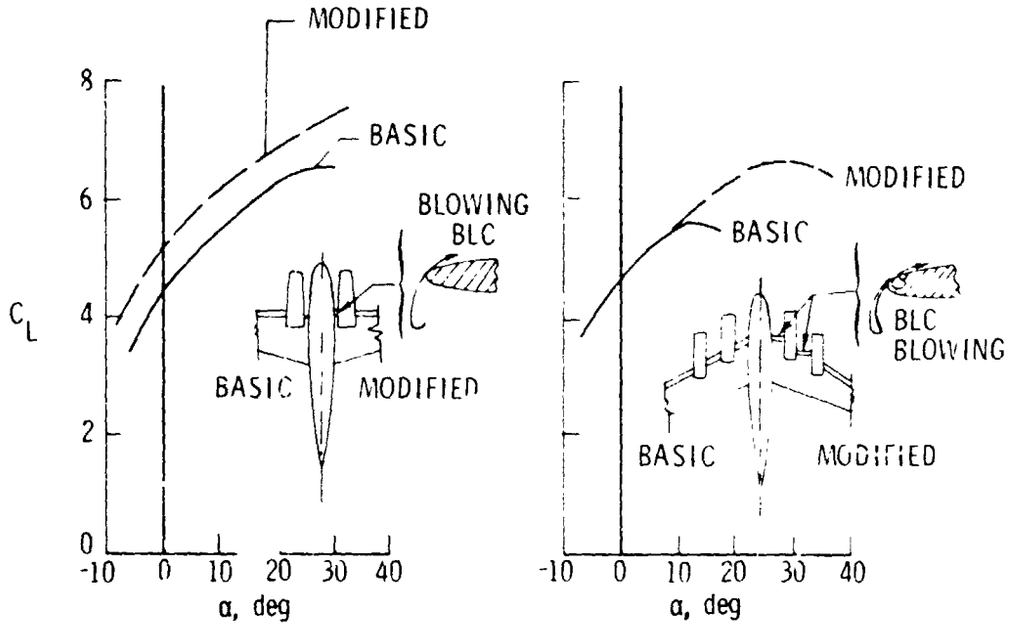

Figure 6.- Leading-edge treatment for two-engine straight-wing and four-engine swept-wing configurations.

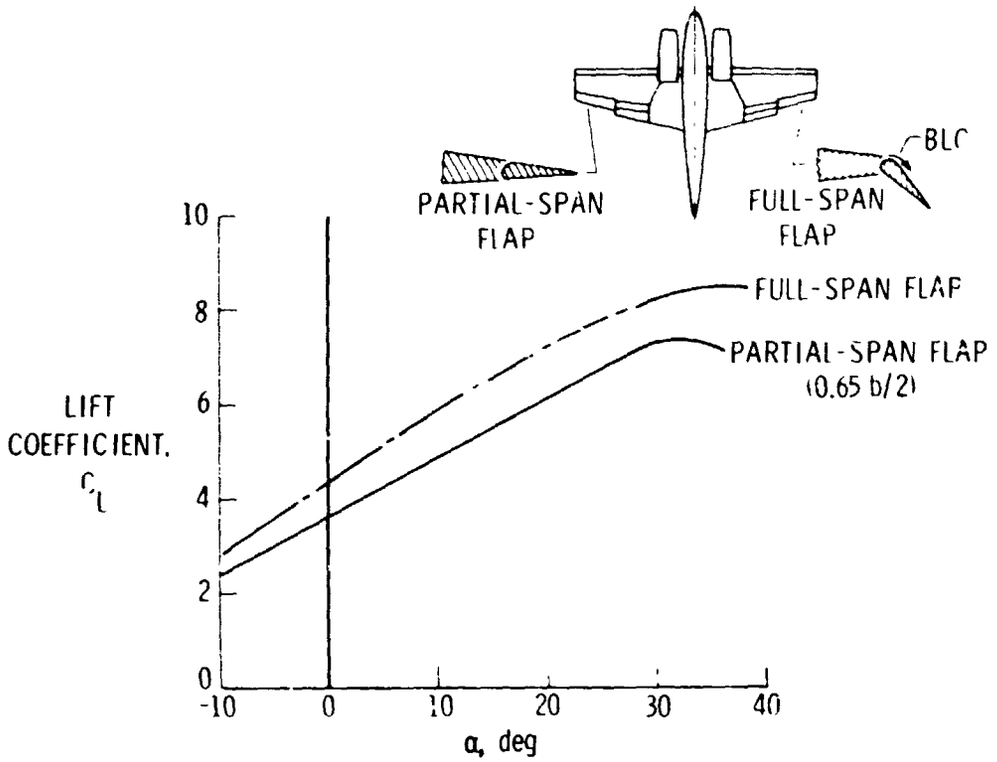

Figure 7.- Effect of trailing-edge flap span on lift. $\delta_f = 60^o$; $C_\mu = 2.0$.

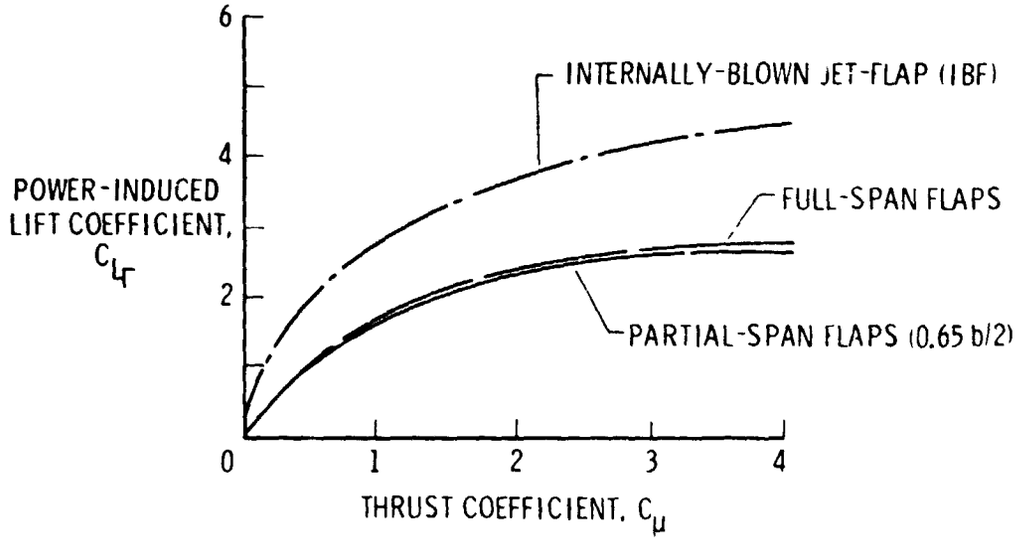

Figure 8.- Power-induced lift characteristics of two-engine straight-wing USB configuration. $\delta_f = 60^o$; $\alpha = 0^o$.

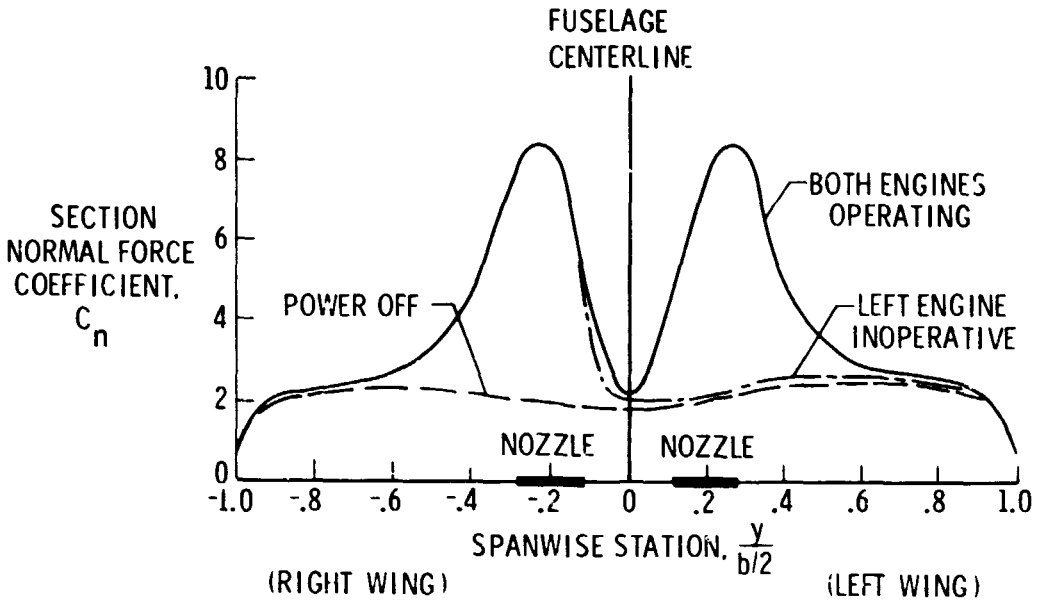

Figure 9.- Spanwise normal-force distribution for two-engine straight-wing USB configuracion. $\delta_f = 60^o$; $\alpha = 0^o$.

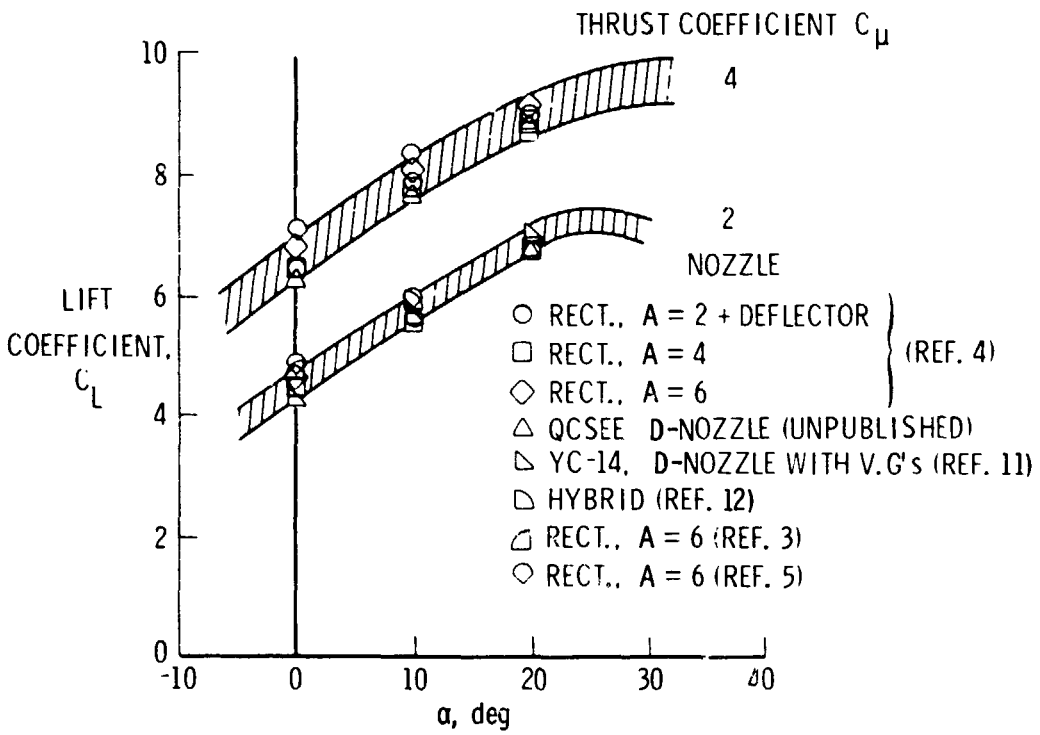

Figure 10.- Effect of nozzle geometry on lift for a number of USB configurations.

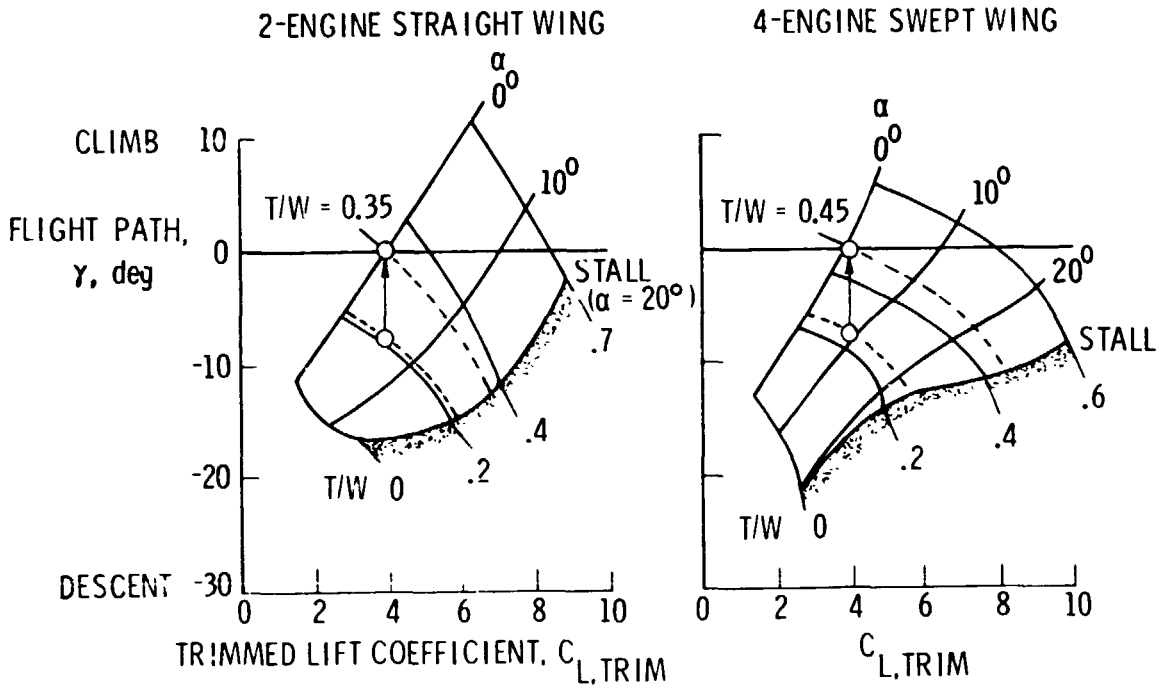

Figure 11.- Flight envelopes for two-engine straight-wing and four-engine swept-wing configurations.

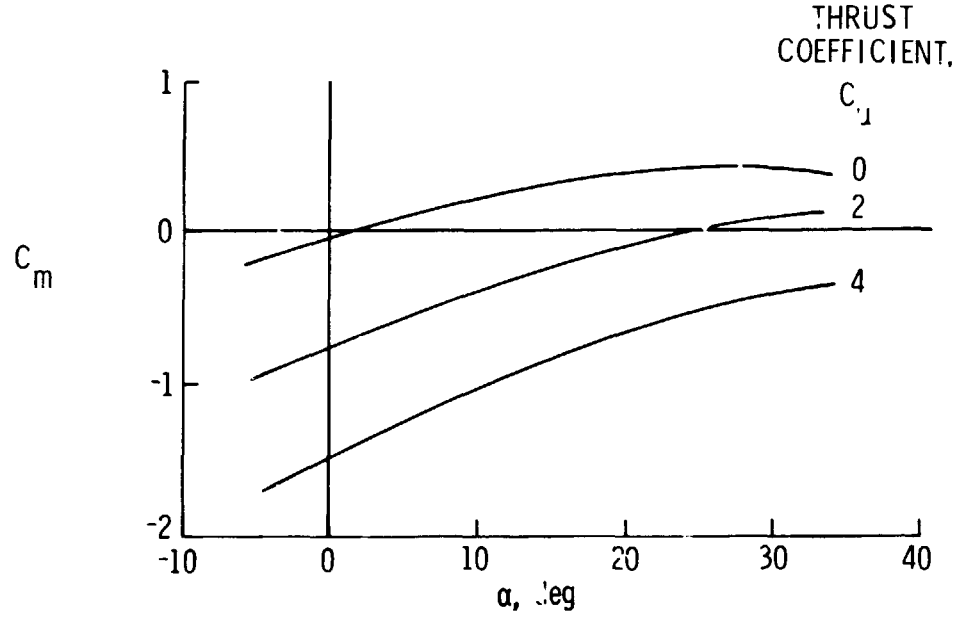

Figure 12.- Tail-off pitching-moment characteristics for four-engine swept-wing configuration. $\delta_f = 65^o$; tail off.

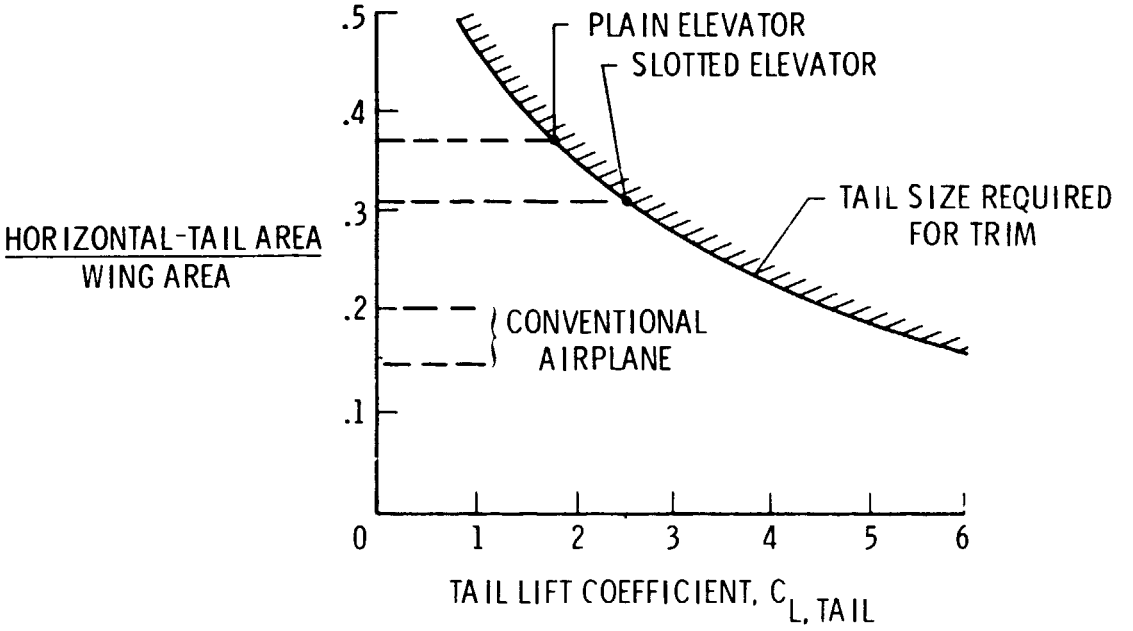

Figure 13.- Horizontal-tail requirements. $C_{L,wing} = 8.0$; $l_t = 3.5\bar{c}$; 10-percent static margin.

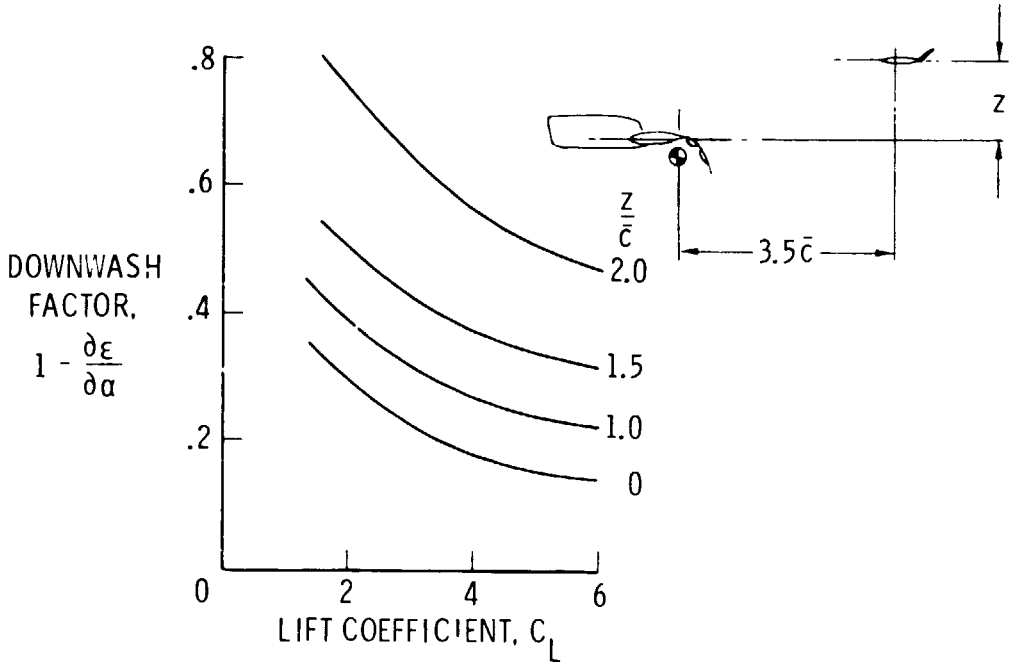

Figure 14.- Variation of downwash factor. $\delta_f = 69^o$.

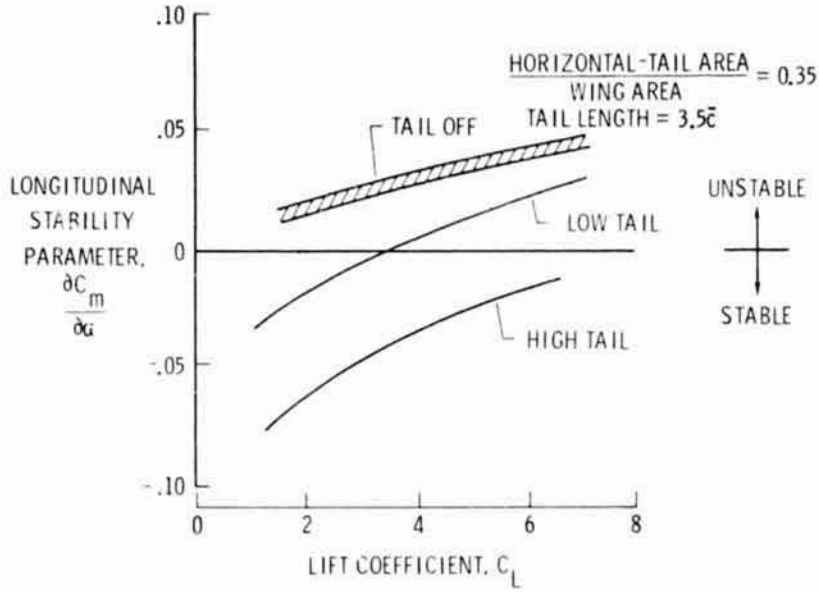

Figure 15.- Static longitudinal stability.

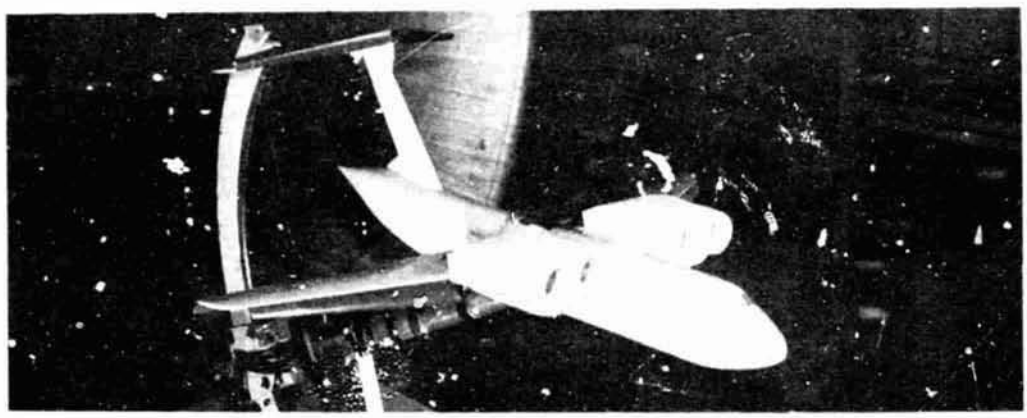

Four-engine swept wing

Two-engine straight wing

Figure 16.- Photographs of two-engine and four-engine USB models installed in the Langley full-scale tunnel.

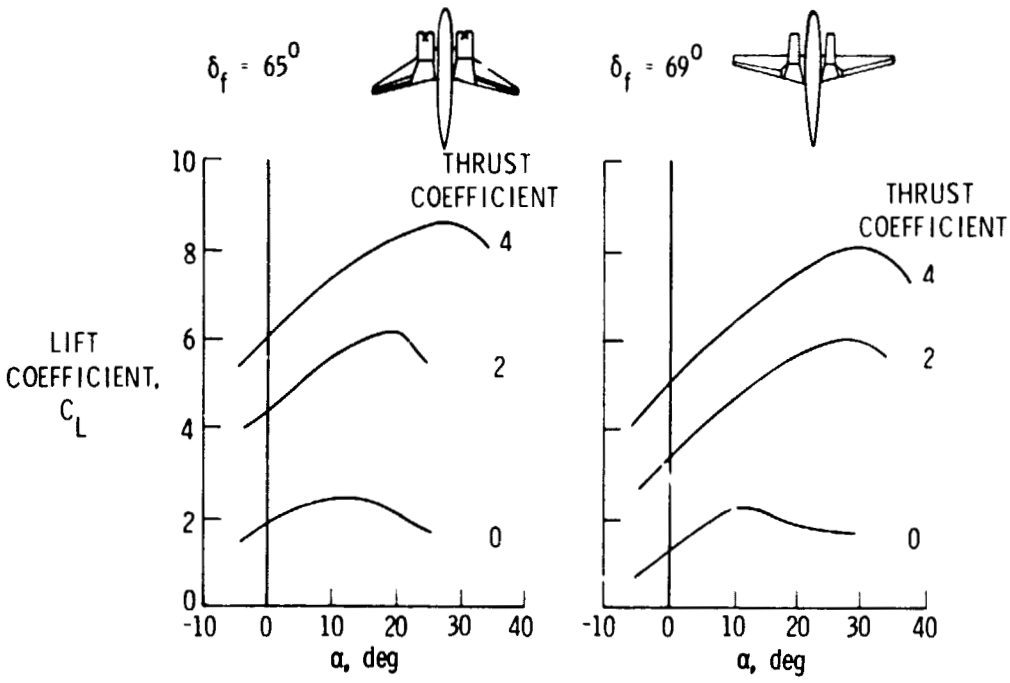

Figure 17.- Lift characteristics of two-engine and four-engine USB models.

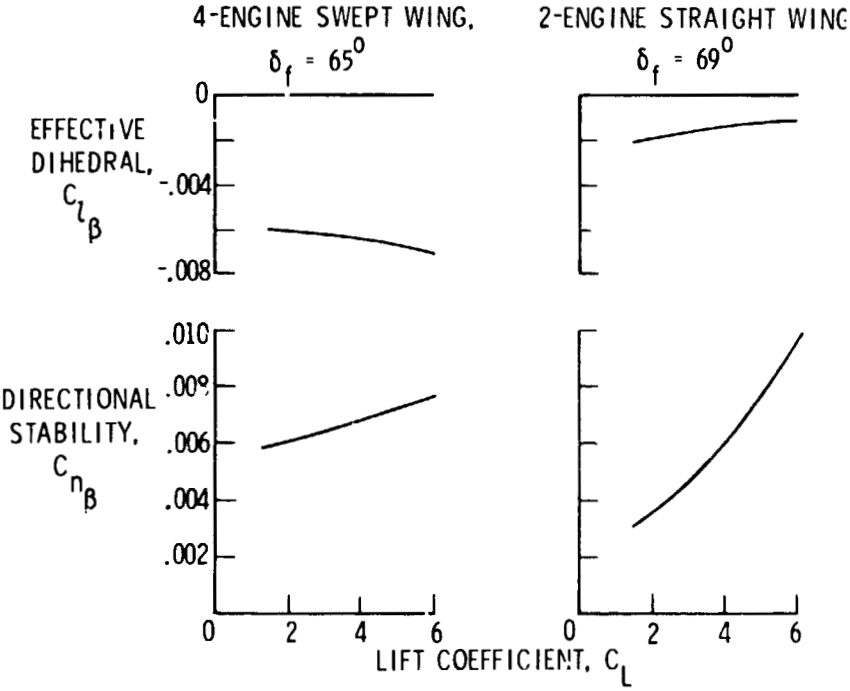

Figure 18.- Lateral-directional stability characteristics of two-engine and four-engine USB models.

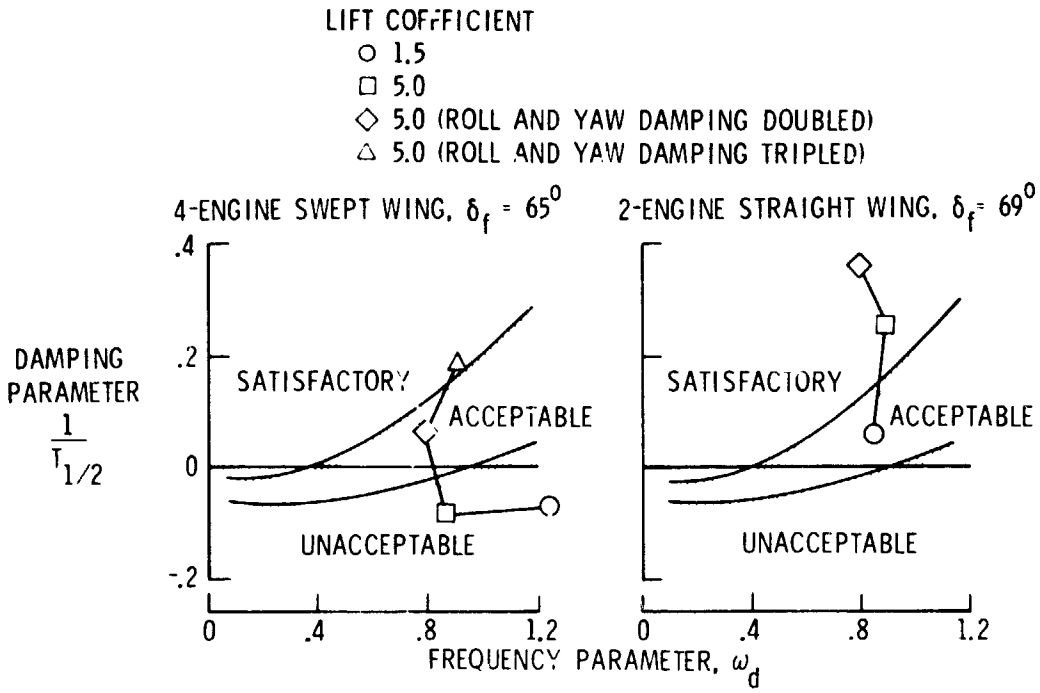

Figure 19.- Dutch-roll characteristics of two-engine and four-engine USB models.

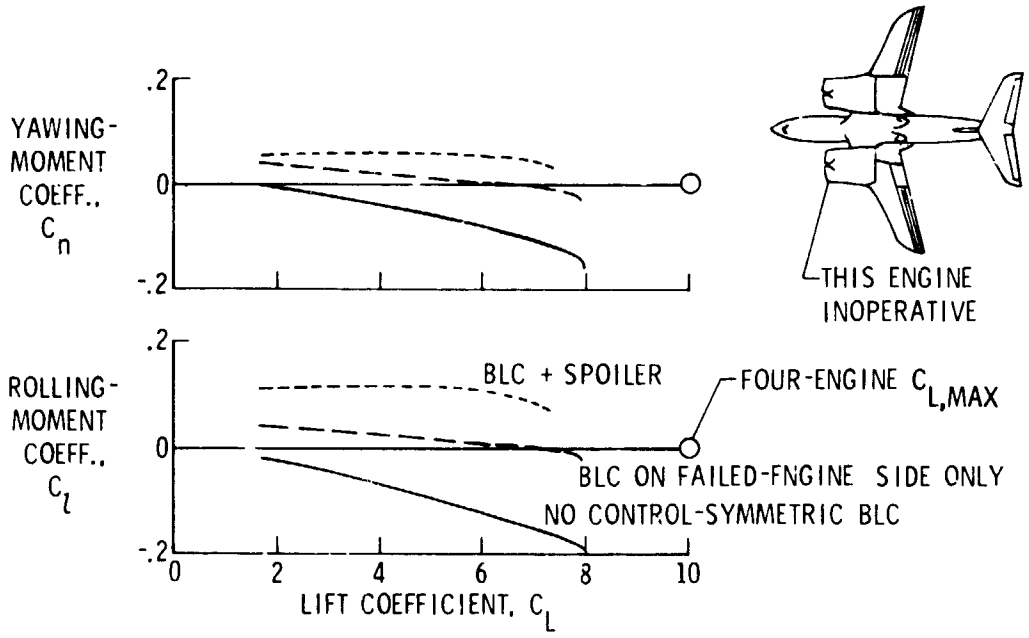

Figure 20.- Lateral trim characteristics for four-engine swept-wing USB model.

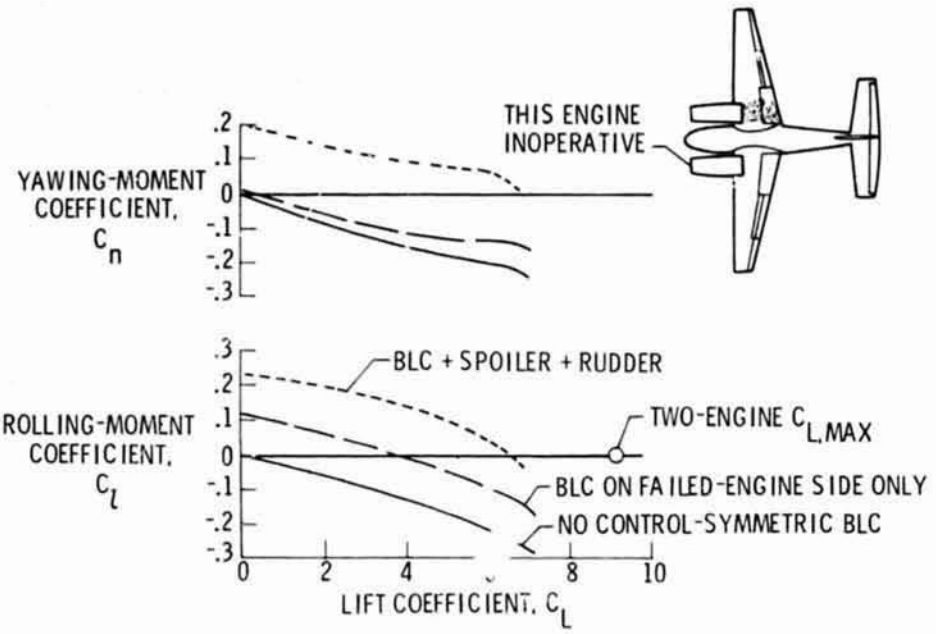

Figure 21.- Lateral trim characteristics for two-engine straight-wing USB model.

Figure 22.- Photograph of four-engine swept-wing free-flight USB model in the Langley full-scale tunnel.

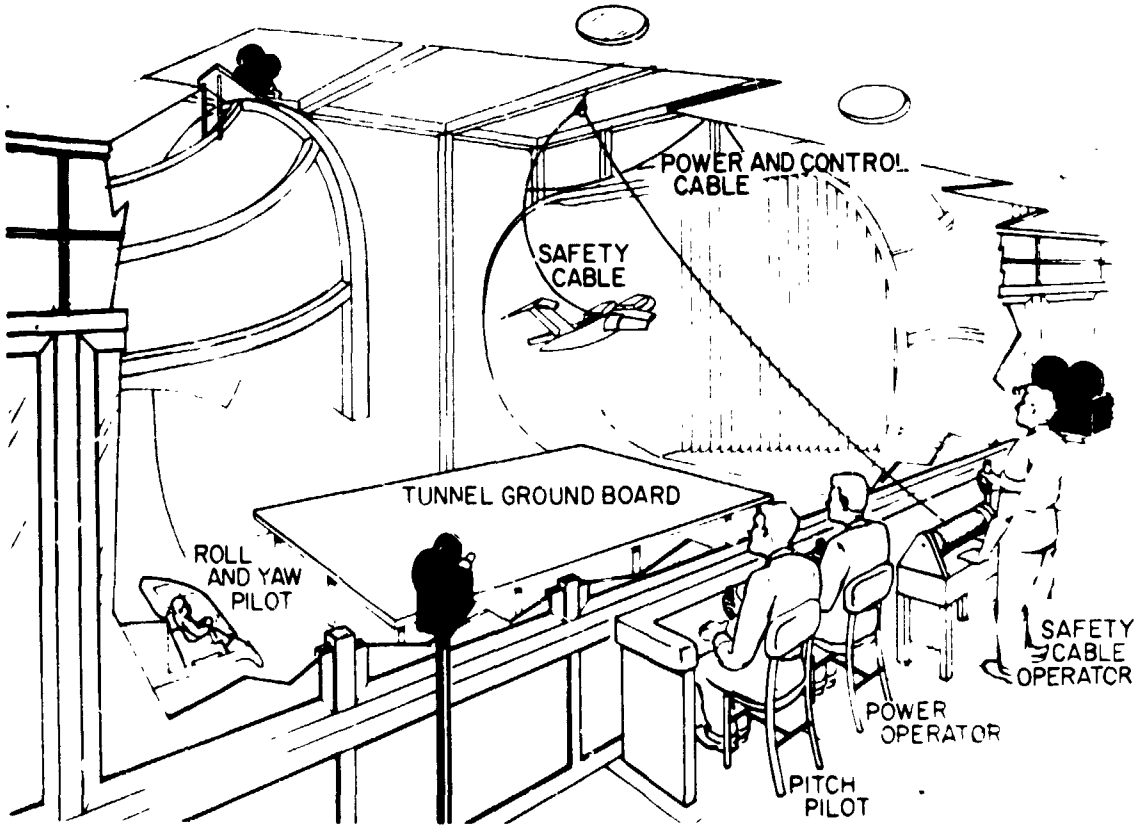

Figure 23.- Test setup for free-flight model testing in the Langley full-scale tunnel.